LASER INTERFEROMETER GRAVITATIONAL WAVE OBSERVATORY
- LIGO -
CALIFORNIA INSTITUTE OF TECHNOLOGY
MASSACHUSETTS INSTITUTE OF TECHNOLOGY

Technical Note	**LIGO-T1500559–v3**	2015/12/02

Frequency response of the aLIGO interferometer: part 3

Kiwamu Izumi, Daniel Sigg and Keita Kawabe
for the aLIGO ISC group

Distribution of this document:

LIGO VIRGO scientific collaboration, and public

California Institute of Technology
LIGO Project, MS 100-36
Pasadena, CA 91125
Phone (626) 395-2129
Fax (626) 304-9834
E-mail: info@ligo.caltech.edu

Massachusetts Institute of Technology
LIGO Project, NW22-295
Cambridge, MA 02139
Phone (617) 253-4824
Fax (617) 253-7014
E-mail: info@ligo.mit.edu

LIGO Hanford Observatory
PO Box 159
Richland, WA 99352
Phone (509) 372-8106
Fax (509) 372-8137
E-mail: info@ligo.caltech.edu

LIGO Livingston Observatory
19100 LIGO Lane
Livingston, LA 70754
Phone (225) 686-3100
Fax (225) 686-7189
E-mail: info@ligo.caltech.edu

http://www.ligo.caltech.edu/

Contents

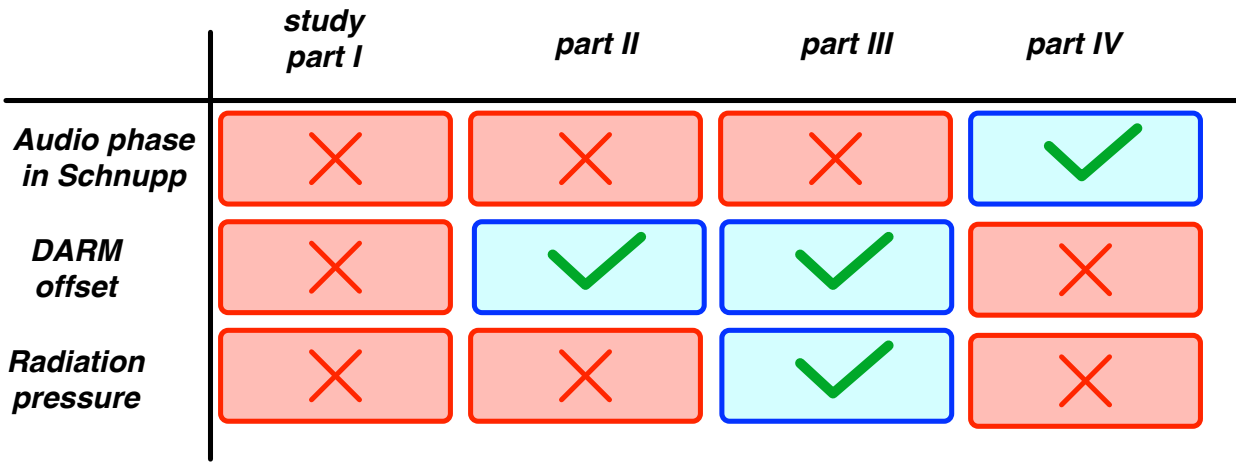

Figure 1: The (tetative) plan of the study. We plan to proceed with four steps. A red box indicates that the corresponding effect is not included while the blue boxes for the included.

1 Overview

1.1 Overview of the whole study

A goal of this study is to deliver clear and accurate picture of how we sense and control the length degrees of freedom (DOFs). For this purpose, we attempt to write down relevant interferometric signals as frequency responses in analytic form which should make underlying physics more apparent. We will intentionally start from a simple configuration and gradually add a few realistic complexities to our model as illustrated in figure 1. Throughout the study, we assume the electric fields to be plane-waves which propagate between well-aligned optics. Therefore neither mode-matching nor misalignment effects are considered.

1.2 Overview of this particular document

This document summarizes the third part of the study. As shown in figure 1, the results presented in this document include the effect of the DARM offset (see more details in [2]) and the radiation pressure. The radiation pressure effect has been newly introduced in this part of the study. The outline of this document is as follows. In section 2, we briefly review how to handle the radiation pressure effect and describe what physics are ignored. In section 3, we compute intensity variation in the arm cavities which is a key point of this study because it is consequently going to displace the arm lengths through the radiation

pressure force. In section 4, we discuss the frequency responses at the AS port with the DC readout. In section 5, we discuss the coupling of laser noises to the AS port in the presence of the radiation pressure. Finally, we conclude this study in section 6 with some remarks for the next step. The definitions of quantities and calculation method can be found in the previous documents [1, 2].

2 Approach

2.1 Overview of the calculation process

To properly include the radiation pressure effect within the frame work of the perturbative sideband technique [4], we proceed with the following steps. First, we excite a degree-of-freedom of interest. This will create a pair of audio sidebands around the carrier and rf sidebands. Second, we compute the intensity variation of the field incident upon the test masses. This in turn informs us about how much radiation pressure is being applied to the test masses and therefore about their displacements. Third, since we are particularly interested in the coupling to DARM, we extract the differential component of the displacement that are driven by the radiation pressure. Finally, propagating the radiation-pressure-driven DARM displacement through the DARM$\rightsquigarrow$ASDC transfer function [2], we evaluate the coupling to the AS DC readout. In the process, we have ignored radiation-pressure-driven-displacement in the MICH degree-of-freedom because the coupling is much smaller than the DARM by approximately a factor of 280 in the case of aLIGO.

2.2 Assumptions

In the analytic calculation, we assume the followings. We assume that the radiation pressure is prominent only on the test masses. Therefore we omit the effect on the rest of mirrors, such as BS, PRM and SRM. In contrast, Optickle [3] computes the radiation pressure on every suspended mirror.

We also assume that variation in the intracavity power of an arm will simultaneously exert an equal amount of radiation pressure force on ITM and ETM. In other words, we do not

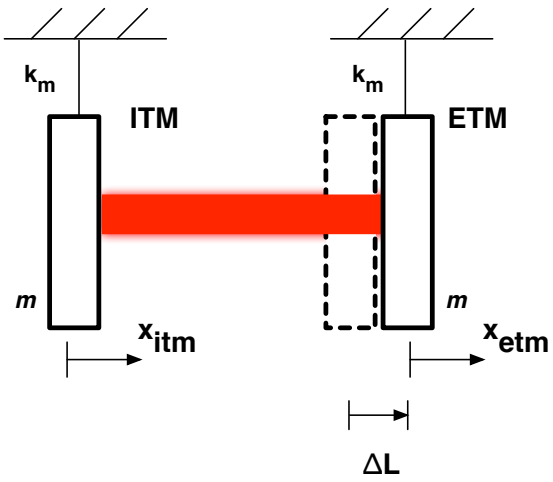

Figure 2: A suspended Fabry-Perot cavity. Each mirror is suspended with a mechanical spring constant of k_m. The mass of each mirror is m. The cavity length is adjusted such that it is displaced from the exact resonance by ΔL.

consider the delay of the propagation of the light and also assume the radiation pressure force to be that for a perfect reflector on each test mass (i.e. $F = 2P/c$ on each test mass). We will come back to this argument in the next subsection with a more concrete example.

Also, the optical spring effect is omitted. This is further discussed in the following subsection.

When computing the signal at the AS DC readout, we ignore the coupling from MICH because the coupling is always smaller than that of DARM.

2.3 Ignorance of the optical spring

In this study, we ignore the optical spring effect because it is not straightforward to handle them in an analytic framework. This will produce a large discrepancy between the full rigorous calculation and our analysis below the opto-mechanical resonance frequency which are numerically found to be as high as 10 Hz when $P_{\rm in} = 125$W with a DARM offset of 5 pm. In the rest of this subsection, we show a simple example to give an idea of how we drop the optical spring effect.

Let us think about a suspended single Fabry-Perot cavity. The setup is shown in figure 2.

In this case, the reaction of the system against external forces can be summarized as follows,

$$\begin{bmatrix} x_{\mathrm{etm}} + x_{\mathrm{itm}} \\ x_{\mathrm{etm}} - x_{\mathrm{itm}} \end{bmatrix} = \begin{bmatrix} 1/\left(k_m - m\omega^2\right) & 0 \\ 0 & 1/\left(k_m + 2k_{\mathrm{opt}} - m\omega^2\right) \end{bmatrix} \begin{bmatrix} F_{\mathrm{etm}} + F_{\mathrm{itm}} \\ F_{\mathrm{etm}} - F_{\mathrm{itm}} \end{bmatrix}, \tag{1}$$

where k_{opt} is the optical spring coefficient. It is generally a function of frequency ω as

$$k_{\mathrm{opt}}(s) = \frac{4\mathcal{F}g^2k^2}{c\left(1+s_{\mathrm{c}}\right)^2}\Delta L, \tag{2}$$

with $\mathcal{F}$ being the finesse coefficient defined by $\mathcal{F} = 4r_{\mathrm{i}}r_{\mathrm{e}}/(1-r_{\mathrm{i}}r_{\mathrm{e}})^2$, g being the cavity amplification coefficient defined by $g = t_{\mathrm{i}}/(1-r_{\mathrm{i}}r_{\mathrm{e}})$ and s_{c} being $i\omega/\omega_{\mathrm{c}}$ where ω_{c} is the cavity pole. In this analysis, we have ignored radiation pressure on the non-cavity side of ITM for simplicity. Notice that the optical spring coefficient vanishes when no length offset is applied i.e. $\Delta L = 0$ as expected. Those who seek more details can look up the excellent references [5, 6].

For our purpose, we do not care the top row of equation (1) because the radiation pressure of the intracavity field is differential on the mirrors. Focusing on the bottom row instead, one can find the simple relation,

$$(\text{net length variation}) = \frac{F_{\mathrm{etm}} - F_{\mathrm{itm}}}{k_m + 2k_{\mathrm{opt}} - m\omega^2}. \tag{3}$$

As stated in the previous subsection 2.2, the radiation pressure force is assumed to be simultaneously exerted on ITM and ETM with the same amplitude. Paying attention to the relative sign between F_{etm} and F_{itm}, one can arrive at

$$(\text{net length variation}) = \frac{2F_{\mathrm{etm}}}{k_m + 2k_{\mathrm{opt}} - m\omega^2}. \tag{4}$$

Since calculating k_{opt} in the full interferometer requires an additional effort to opto-mechanically relate every mirror to the others, we purposely avoid such a laborious task by applying a high frequency limit, $m\omega^2 \gg |k_m + 2k_{\mathrm{opt}}|$. Finally, using the basic radiation pressure formula of

$F_{\rm etm} = 2\Delta P/c$ with ΔP being a small deviation in the cavity power, one can obtain,

$$(\text{net length variation}) = -\frac{4\Delta P}{cm\omega^2}, \tag{5}$$

This approximation allows us to skip the calculation of $k_{\rm opt}$ at the expense of accuracy in the frequency where the condition $m\omega^2 \leq |k_m + 2k_{\rm opt}|$ is met.

2.4 Reduced mass

Since we have approximated the mirrors to be free from both mechanical and opto-mechanical restoring forces, it is now only two free masses experiencing the same amount of force. In such a mechanical system, it is often convenient to introduce the reduced mass,

$$\mu = \frac{m_{\rm i} m_{\rm e}}{m_{\rm i} + m_{\rm e}}, \tag{6}$$

where m_i and $m_{\rm e}$ are the mass of ITM and ETM respectively. Using the reduced mass, one can rewrite the reaction equation (5) as

$$(\text{net length variation}) = \frac{2\Delta P}{cs_\mu^2}, \tag{7}$$

where s_μ is a Laplace representation of the mechanical response defined by,

$$s_\mu^2 = -\mu\omega^2. \tag{8}$$

This form is often used in the rest of the document.

2.5 A special case: radiation pressure on ITM

We have so far discussed the radiation pressure due to variation in the intracavity field. However, of course, there may be a case where the radiation pressure on the non-cavity side of ITM matters more than the intracavity. Such a case actually exists when one considers the rf sidebands because they are not resonant in the arms and hence naturally larger radiation pressure on the non-cavity side.

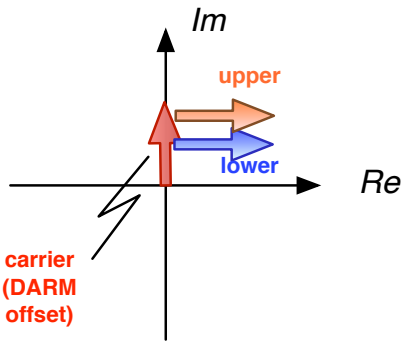

Figure 3: A phaser representation of the SRC intracavity field. It has a static carrier field pointing alog the imaginary axis or phase quadrature. An excitation in SRCL imposes a pair of audio sidebands which point along the real axis or amplitude quadrature.

When the ITMs are differentially displaced by radiation pressure of the rf sidebands, it is going to displace both DARM and MICH degrees-of-freedom simultaneously. However, we ignore the displacement of MICH for the same reason as stated in section 2.1. In addition, we approximate the resultant intensity-to-displacement relation to be half of equation (7), so that

$$(\text{net length variation}) = -\frac{\Delta P^{(\text{ITM, AR side})}}{cs_\mu^2}. \tag{9}$$

Pay attention to the sign – a positive force shrinks the length of the cavity and hence an extra minus sign in front. This equation will be used only once in section 5.4.

3 Intensity variation in the arm cavities

Calculating the intensity variation around the arm cavities is vital for modeling the radiation pressure effect. In this section, we compute the transfer function from various excitation points (e.g. PRCL and SRCL displacements, frequency noise and etc.) to the intensity variation in the arm cavities. In addition, we compute a transfer function from oscillator phase noise to the intensity variation of the rf sidebands on the AR side of ITMs.

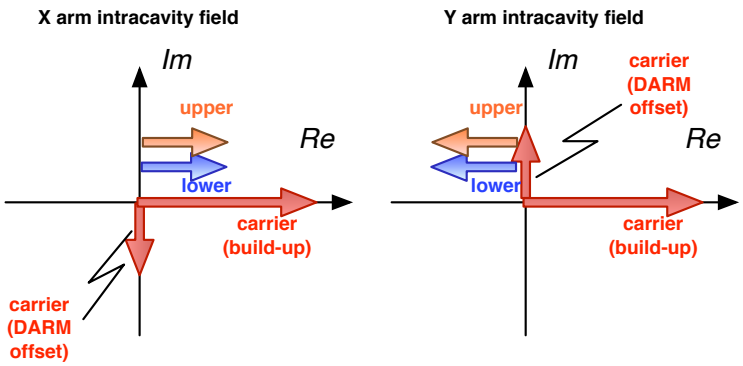

Figure 4: A phaser representation of the intracavity field of the arm cavities. See the main body for explanations.

3.1 SRCL excitation to arms' intensity

Prior to working out some algebra, we attempt to explain why the SRCL degree-of-freedom easily excites the intensity in the arms by using a phaser diagram. Figure 3 shows the signal recycling cavity field in phaser diagram. It contains a carrier static offset pointing along the imaginary axis or phase quadrature. This static carrier is given by the DARM offset and therefore would vanish if no DARM offset was applied. When SRCL is excited in its length, it is going to impose phase-modulation sidebands on the static carrier. In the phaser representation, it is equivalent to add a pair of the audio sidebands pointing along the real axis or amplitude quadrature. At this point, this does not create an observable signal at the AS DC readout because the imposed sidebands do not change the intensity of the static carrier field. In other words, the sidebands are orthogonal to the DARM offset field.

However, when the sidebands propagate to the arm cavities, an interesting thing happens. Figure 4 shows the intracavity field of the arms in phaser diagram. Besides the audio sidebands, the intracavity fields are composed of two components – the build-up and DARM offset fields. As shown in the figure, both arms have a large build-up field along the real axis. Their sizes are very large because of the combination of the power recycling and resonating arms. As we introduce a small DARM offset in the lengths, it is going to add a small imaginary part which has the same size between two arms but with the opposite sign. Finally, the excited sidebands come into the arms by bouncing back from SRM and impose a pair of the sidebands pointing along the real axis. Notice that the direction of where the audio sideabands point at is opposite between two arms because of the reflection-transmission

relation on the beam splitter. Obviously such sidebands can now directly change the size of the static build-up field because they point to the same direction. This causes a differential intensity variation in two arms.

In the rest, we derive an analytic expression for the intensity variation driven by SRCL. A small change in the signal recycling cavity field $\Delta E_{\rm s}$[1] will cause a small change in the intracavity field of X and Y arms by $\Delta E_{\rm x}$ and $\Delta E_{\rm y}$ respectively. They can be found as,

$$\frac{\Delta E_{\rm x}}{\Delta E_{\rm s}} = +i\frac{g g_{\rm s} r_{\rm s}}{\sqrt{2}t_{\rm s}\left(1+s_{\rm rse}\right)}, \quad \frac{\Delta E_{\rm y}}{\Delta E_{\rm s}} = -i\frac{g g_{\rm s} r_{\rm s}}{\sqrt{2}t_{\rm s}\left(1+s_{\rm rse}\right)}, \tag{10}$$

where g is arm's amplitude amplification coefficient given by $g = t_{\rm i}/(1-r_{\rm i}r_{\rm e})$. As discussed earlier with the phaser diagram, the relative sign between two transfer functions differ due to the reflection-transmission relation of the beam splitter. We have omitted the effect of the DARM offset because it is insignificant.

When SRCL is excited by $\Delta l_{\rm s}$ at a frequency ω, it scatters the carrier static field to frequency components at $\omega_0 \pm \omega$ with an additional amplitude coefficient of $-ik\Delta l_{\rm s}$. The intracavity field of the signal recycling cavity is now written as

$$E_{\rm s} = E_{\rm s}^{(\rm static)} e^{i\omega_0 t}\left(1 - ik\Delta l_{\rm s} e^{i\omega t} - ik\Delta l_{\rm s} e^{-i\omega t}\right). \tag{11}$$

This is just a repeat of what Regehr describes in [4]. The second and third terms are the upper and lower audio sidebands around the carrier field respectively. These two terms correspond to the small deviation $\Delta E_{\rm s}$ in equation (10). Plugging the above equation to equation (10), one can find,

$$\Delta E_{\rm x}\left(\omega\right) = \sqrt{2}\frac{J_0 g g_{\rm p} g_{\rm s}^2 r'_{\rm a} r_{\rm s}\epsilon}{t_{\rm s}^2\left(1+s_{\rm rse}\right)} E_{\rm in} k\Delta l_{\rm s} e^{i\omega t}. \tag{12}$$

where we have substituted $E_{\rm s}^{(\rm static)} = 2J_0 g_{\rm p} g_{\rm s} r'_{\rm a}\epsilon E_{\rm in}/t_{\rm s}$. This field then interferes with the

[1] $E_{\rm s}$ represents a field incident on SRM. This field is rotated by $-i$ from that shown in figure 3 because of the SRC resonance condition.

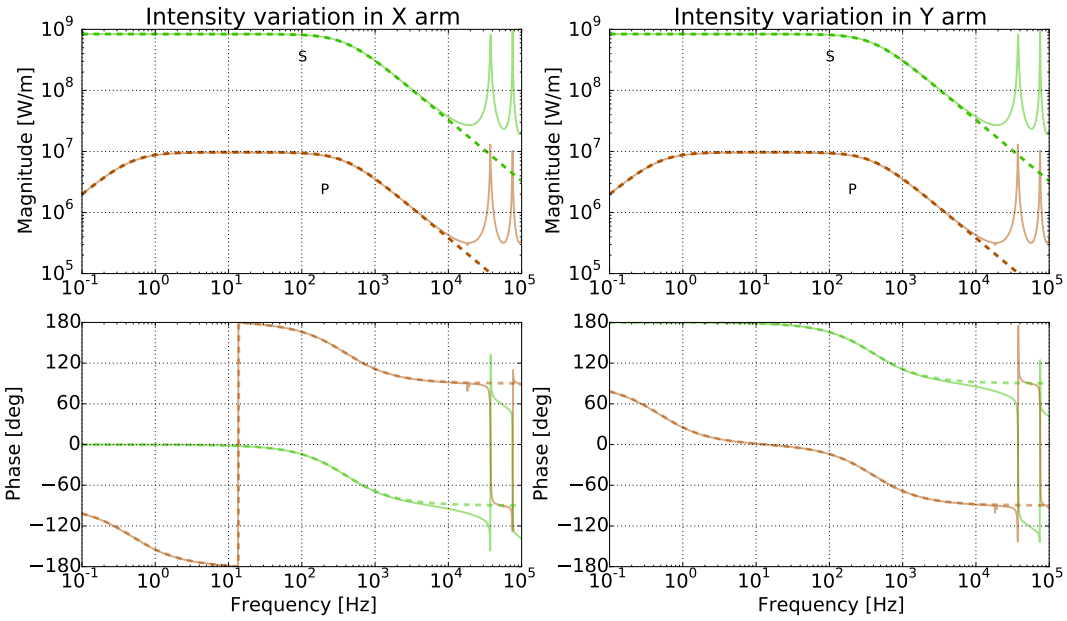

Figure 5: Intensity variation in X arm (left) and Y arm (right). The dashed lines are the responses derived by the analytic approach. The solid lines are that from Optickle [3]. The lines annotated with **S** represents that from SRCL and **P** for that from PRCL. All the curves are normalized by $P_{\rm in}$. No opto-mechanical interactions are included in Optickle for this particular computation. No arm imbalances are introduced.

static carrier field in the X arm which is

$$E_{\rm x}^{\rm (static)} = \frac{J_0}{\sqrt{2}} g g_{\rm p} E_{\rm in}. \tag{13}$$

Again, we have omitted the DARM offset ϵ here according to the reasons discussed in the phaser analysis.

Now we compute the intensity variation in the X arm by combining equations (12) and (13) via equation (9) of [2]. It will give us,

$$\Delta P_{\rm x} = +\frac{8 P_{\rm a} g_{\rm s}^2 r_{\rm s} r'_{\rm a} \epsilon}{t_{\rm s}^2 \left(1 + s_{\rm rse}\right)} k \Delta l_s, \tag{14}$$

where $P_{\rm a}$ is the laser power stored in an arm cavity defined as $P_{\rm a} = (J_0 g_{\rm p} g)^2 |E_{\rm in}|^2/2$. Simi-

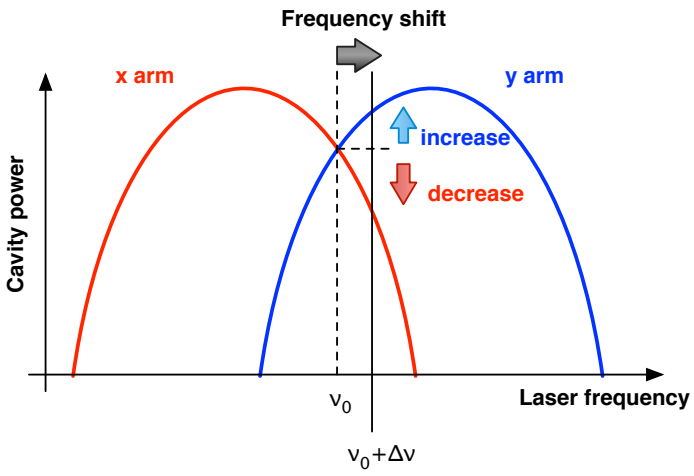

Figure 6: Frequency fluctulation excites differential intensity variation.

larly, one can obtain that for the Y arm as,

$$\Delta P_{\rm y} = -\frac{8 P_{\rm a} r'_{\rm a} \epsilon g_{\rm s}^2 r_{\rm s}}{t_{\rm s}^2 \left(1 + s_{\rm rse}\right)} k \Delta l_s. \tag{15}$$

It is clear that the intensity variation are differential between two arms. As shown in figure 5, the analytic expressions show a good agreement with the full numerical simulation by Optickle. This differential radiation pressure drives DARM and consequently produces signals at the AS DC.

3.2 Frequency noise to arms' intensity

Here, we discuss $\Delta f \rightsquigarrow \Delta P_{\rm x,y}$ transfer functions. Figure 6 illustrates the coupling mechanism. As shown in the cartoon, two arms are offset from the exact operating point by an equal amount but with the opposite sign due to the DARM offset. The laser frequency nominally should be at the point where the cavity power of two arms are identical. When the frequency of the laser shifts by a small amount of Δf, it decreases the cavity power of the X arm while the Y arm increases or vice versa. This is a different coupling mechanism than the $\Delta l_{\rm s} \rightsquigarrow \Delta P$ coupling.

Now, let us work out a bit on some algebra. In the steady state, the transfer function from

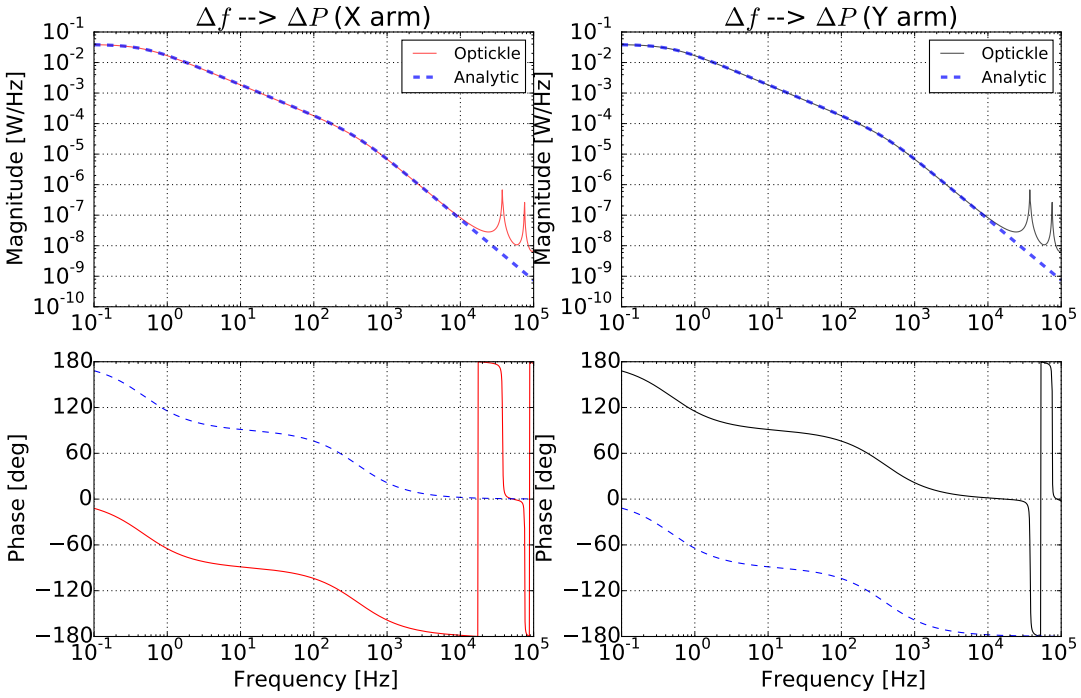

Figure 7: Intensity variation in X arm (left) and Y arm (right) when frequency noise at the input field is excited. The dashed lines are the responses derived by the analytic approach. The solid lines are that from Optickle [3]. All the curves are normalized by $P_{\rm in}$. No opto-mechanical interactions are included in Optickle for this particular computation. No arm imbalance is introduced in either the numerical simulation or analytic expressions.

input field to the intracavity field of each arm can be written as

$$\frac{E_{\rm x}}{E_{\rm in}} = \frac{1}{\sqrt{2}}\frac{g g_{\rm p}}{1+s_{\rm cc}}\left(1 - i\epsilon\frac{g_{\rm s}^2 r'_{\rm a}}{1+s_{\rm rse}}\right), \quad \frac{E_{\rm y}}{E_{\rm in}} = \frac{1}{\sqrt{2}}\frac{g g_{\rm p}}{1+s_{\rm cc}}\left(1 + i\epsilon\frac{g_{\rm s}^2 r'_{\rm a}}{1+s_{\rm rse}}\right). \tag{16}$$

The two transfer functions are similar but there is a sign difference in the first order term for the DARM offset ϵ. Using equation (9) and table 1 of [2] , one can find the intensity variation as

$$\Delta P_{\rm x} = -\Delta P_{\rm y} = -4\pi\frac{P_{\rm a} g_{\rm s}^2 r'_{\rm a}\epsilon}{J_0\omega_{\rm rse}\left(1+s_{\rm cc}\right)\left(1+s_{\rm rse}\right)}\Delta f. \tag{17}$$

Figure 7 shows a comparison between the above expression against Optickle. Currently there is a sign difference between the numerical simulation and analytic expressions for unknown reason. According to the simple analysis illustrated in figure 6, the transfer function for the X arm should start from 180 degrees in its phase at DC and therefore something must be

wrong in the way we set up the numerical simulation.

3.3 PRCL excitation to arms' intensity

When PRCL is excited, it is going to phase-modulate the field incident on the beam splitter. Therefore this is similar to the Δf coupling. Working out some algebra, one can find the intensity variation of the arms to be

$$\Delta P_{\mathrm{x}} = -\Delta P_{\mathrm{y}} = \frac{2P_{\mathrm{a}}g_{\mathrm{p}}g_{\mathrm{s}}^2 r'_{\mathrm{a}}\epsilon\left(1+r_{\mathrm{a}}r_{\mathrm{p}}\right)s_{\mathrm{rse}}}{t_{\mathrm{p}}\left(1+s_{\mathrm{cc}}\right)\left(1+s_{\mathrm{rse}}\right)}k\Delta l_p. \tag{18}$$

These transfer functions are shown in figure 5 in bode plot together with the ones from Optickle. The analytic expression agrees with Optickle. Even though the coupling mechanism of the Δl_{p} excitation is similar to that of Δf, there is a fundamental difference between them. While Δl_{p} excites the phase of the field incident on the beam splitter, Δf excites the frequency of the field. From the fundamental relation between phase and frequency i.e. $\Delta\phi = \Delta\nu/(if)$, one can expect the difference to be $1/f$ in their transfer function shapes. Indeed this difference exists. The Δl_{p} transfer function has an extra zero at DC compared to the Δf.

3.4 Laser intensity to arms' intensity

Now we consider the coupling of the amplitude or intensity of the input field. As it turns out, the intensity variation of the arm cavities will be mostly common between two arms. However at the same time, it leaves small differential components depending on the imbalance between two arms.

Solving the interferometer matrix in the steady state, one can obtain the following propaga-

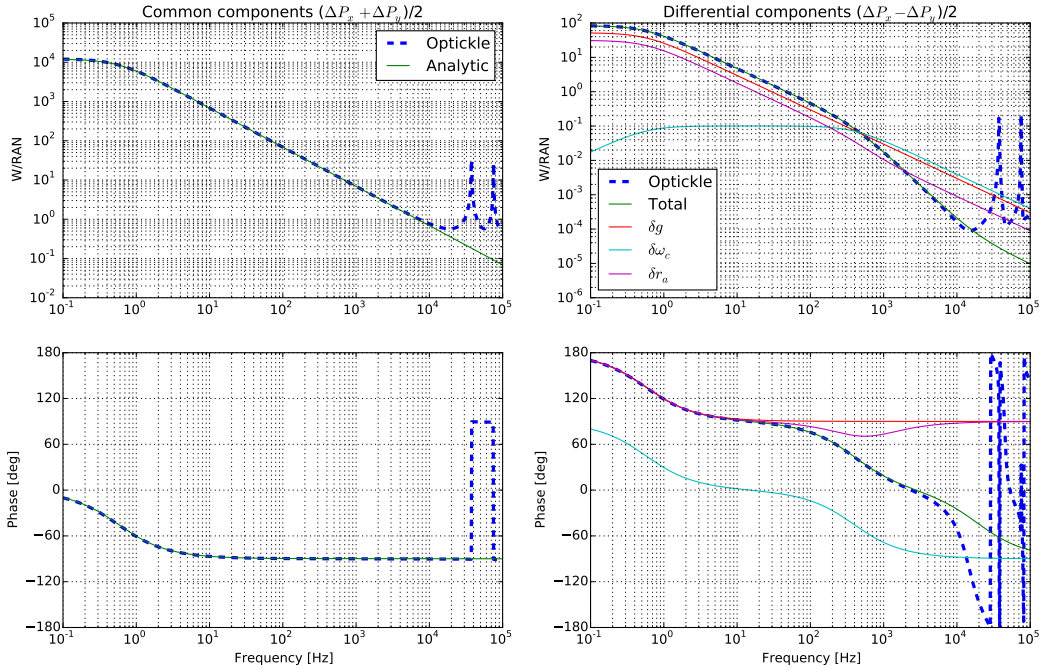

Figure 8: Couplings from amplitude excitation $\Delta A/A$ to common (left) and differential (right) components of arms' intensity. No opto-mechanical interaction is included in Optickle. All the transfer functions are normalized by the input power $P_{\rm in}$.

tion relations of the input field,

$$\begin{aligned}
\frac{E_{\rm x}}{E_{\rm in}} =& \frac{1}{\sqrt{2}}\left[\frac{g}{1+s_{\rm c}} + \frac{\delta g}{1+s_{\rm c}} - \left(\frac{\delta\omega_{\rm c}}{\omega_{\rm c}}\right)\frac{g s_{\rm c}\left(g_{\rm s} r_{\rm a} r_{\rm s} + g_{\rm s} r_{\rm s} - s_{\rm rse} t_{\rm s} - t_{\rm s}\right)}{t_{\rm s}\left(1+s_{\rm c}\right)^2\left(1+s_{\rm rse}\right)}\right.\\
&\left. + \delta r_{\rm a}\frac{g g_{\rm s} r_{\rm s}}{t_{\rm s}\left(1+s_{\rm c}\right)\left(1+s_{\rm rse}\right)}\right],\\
\frac{E_{\rm y}}{E_{\rm in}} =& \frac{1}{\sqrt{2}}\left[\frac{g}{1+s_{\rm c}} - \frac{\delta g}{1+s_{\rm c}} + \left(\frac{\delta\omega_{\rm c}}{\omega_{\rm c}}\right)\frac{g s_{\rm c}\left(g_{\rm s} r_{\rm a} r_{\rm s} + g_{\rm s} r_{\rm s} - s_{\rm rse} t_{\rm s} - t_{\rm s}\right)}{t_{\rm s}\left(1+s_{\rm c}\right)^2\left(1+s_{\rm rse}\right)}\right.\\
&\left. - \delta r_{\rm a}\frac{g g_{\rm s} r_{\rm s}}{t_{\rm s}\left(1+s_{\rm c}\right)\left(1+s_{\rm rse}\right)}\right]
\end{aligned} \tag{19}$$

One can already notice that the first term, which is the leading term, has the identical sign between the two equations, but the rest of the terms have exactly opposite signs. The effect of such sign differences will become clearer when we compute the intensity variation.

Using the last equation, equation (9) and table 1 of [2], one can compute the intensity

variation in the arm cavities as,

$$\begin{aligned}\frac{\Delta P_{\rm x}}{(\Delta A/A)} =& \frac{2P_{\rm a}}{1+s_{\rm cc}}\left[1+\left(\frac{\delta g}{g}\right)+\left(\frac{\delta\omega_{\rm c}}{\omega_{\rm c}}\right)\frac{g_{\rm s}s_{\rm c}\left(1-r_{\rm s}\right)}{t_{\rm s}\left(1+s_{\rm rse}\right)}-\delta r_{\rm a}\frac{g_{\rm s}^2 r_{\rm s}\left(2+s_{\rm rse}\right)}{t_{\rm s}\left(1+s_{\rm rse}\right)}\right]\\ \frac{\Delta P_{\rm y}}{(\Delta A/A)} =& \frac{2P_{\rm a}}{1+s_{\rm cc}}\left[1-\left(\frac{\delta g}{g}\right)-\left(\frac{\delta\omega_{\rm c}}{\omega_{\rm c}}\right)\frac{g_{\rm s}s_{\rm c}\left(1-r_{\rm s}\right)}{t_{\rm s}\left(1+s_{\rm rse}\right)}+\delta r_{\rm a}\frac{g_{\rm s}^2 r_{\rm s}\left(2+s_{\rm rse}\right)}{t_{\rm s}\left(1+s_{\rm rse}\right)}\right].\end{aligned} \tag{20}$$

The first term of two equations represents the primary effect – ΔA primarily causes common intensity variation. In contrast, the rest are all differential. The second term is a differential component due to a difference in the arm cavity gain δg. The third term is another one due to a difference in the cavity pole $\delta\omega_{\rm c}$. The last terms is yet another one which is induced by a difference in arms' reflectivities $\delta r_{\rm a}$. The common and differential components of the above equations are shown in figure 8 together with the one from Optickle for comparison. They show a good agreement.

3.5 Oscillator phase noise to ITM incident field

In this subsection, we compute intensity variation on the AR side of ITMs. We only consider the rf sidebands and only compute that for the 45 MHz sideband for simplicity. A similar effect is expected for the 9 MHz rf sidebands. After some algebra using equation (9) and table 1 of [2], one can find the differential component of the intensity variation on ITMs to be,

$$\frac{\Delta P_{\rm diff}}{\Delta\Phi} = \frac{1}{2}\left(\frac{\Delta P_{\rm IX}}{\Delta\Phi}-\frac{\Delta P_{\rm IY}}{\Delta\Phi}\right) = i\frac{\left(2J_1 g_{\rm sb}t_{\rm sm}\right)^2 r_{\rm s}}{\hat{r_{\rm a}}t_{\rm s}^2\sin\phi_{\rm sch}}\frac{\omega}{c}\left(l_{\rm s}-L\frac{\hat{r_{\rm a}}'}{\hat{r_{\rm a}}}\right)P_{\rm in}. \tag{21}$$

This differential intensity would not happen if the signal recycling mirror was removed. For example, setting $r_{\rm s}\to 0$ will vanish the coupling in the above equation.

4 Frequency responses

We normalize the DC readout responses by $S_1 = 2J_0^2 P_{\rm in}$. In order to verify the analytic equations, we use Optickle this time.

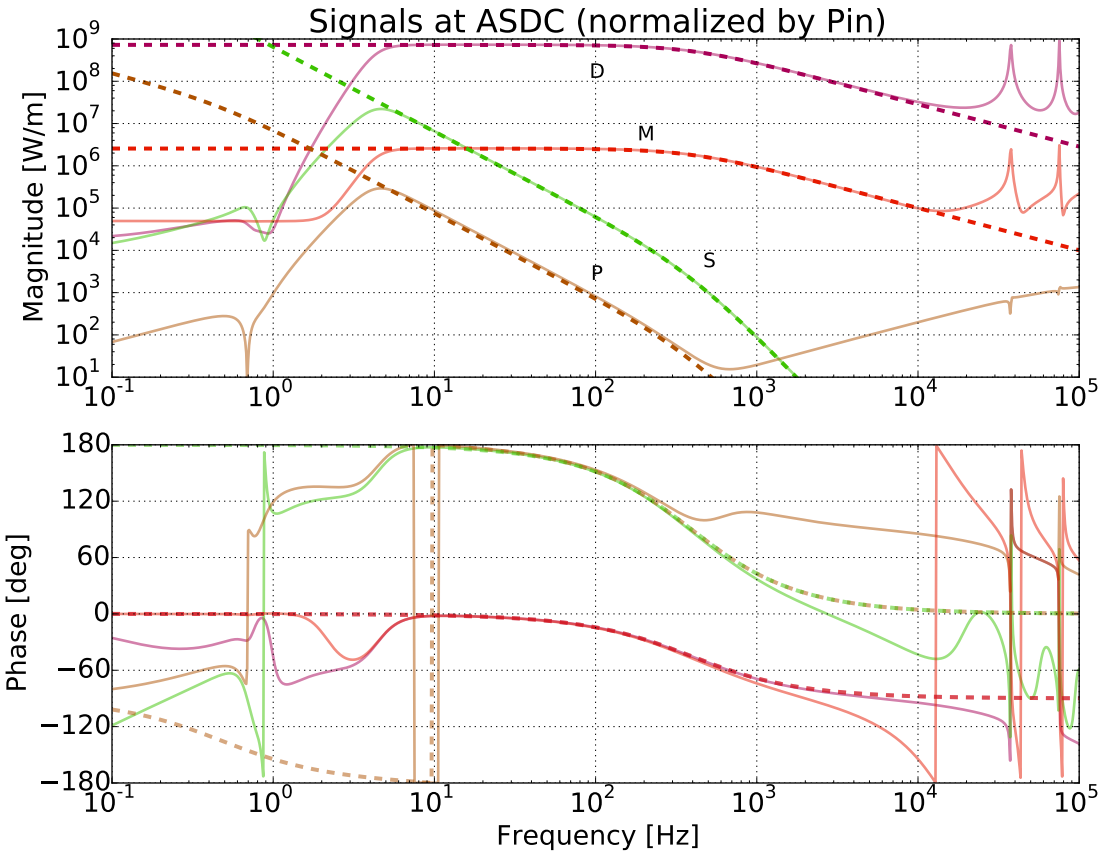

Figure 9: Frequency response at ASDC normalized by $P_{\rm in}$. The dashed lines represent responses derived in the analytic form. The solid lines are the ones numerically computed by Optickle [3]. The annotation letters indicate the following degrees-of-freedom, D; DARM, M; MICH, P; PRCL, S; SRCL. No losses or arm imbalance are applied.

4.1 AS port with DC readout

The response can be summarized as

$$\begin{aligned}\frac{S^{(\rm dc)}}{S_1} =& 4g_{\rm p}^2 g_{\rm s}^2 r_{\rm a}'^2 \epsilon k \Delta L_- \frac{1}{1+s_{\rm rse}} \\ &+ 4g_{\rm p}^2 g_{\rm s}^2 r_{\rm a}' r_{\rm a} \epsilon k \Delta l_- \frac{1}{1+s_{\rm rse}} \\ &+ 4g_{\rm p}^2 g_{\rm s}^2 r_{\rm a}'^2 \epsilon k \frac{1}{1+s_{\rm rse}} \left(\frac{\partial L_-}{\partial l_p}\right) \Delta l_p, \\ &+ 4g_{\rm p}^2 g_{\rm s}^2 r_{\rm a}'^2 \epsilon k \frac{1}{1+s_{\rm rse}} \left(\frac{\partial L_-}{\partial l_s}\right) \Delta l_s.\end{aligned} \tag{22}$$

where $\partial L_-/\partial l_\mathrm{s}$ and $\partial L_-/\partial l_\mathrm{p}$ are opto-mechanical couplings due to the radiation pressure. They are defined as,

$$\begin{aligned}\frac{\partial L_-}{\partial l_p} &= \frac{4 g_\mathrm{p} g_\mathrm{s}^2 r'_\mathrm{a} \epsilon \left(1 + r_\mathrm{a} r_\mathrm{p}\right) s_\mathrm{rse}}{c s_\mu^2 t_\mathrm{p} \left(1 + s_\mathrm{cc}\right)\left(1 + s_\mathrm{rse}\right)} P_\mathrm{a} k, \\ \frac{\partial L_-}{\partial l_s} &= \frac{16 r'_\mathrm{a} \epsilon g_\mathrm{s}^2 r_\mathrm{s}}{c s_\mu^2 t_\mathrm{s}^2 \left(1 + s_\mathrm{rse}\right)} P_\mathrm{a} k.\end{aligned} \tag{23}$$

Figure 9 shows the responses in bode plot. They show good agreement with Optickle above 10 Hz except for high frequency part of PRCL. This is known to be due to the Schnupp asymmetry which is not included in the analytic calculation.

The primary signals – MICH and DARM – scale with the power- and signal- recycled power $P_\mathrm{in} g_\mathrm{p}^2 g_\mathrm{s}^2$ and DARM offset ϵ. On the other hand, the coupling of PRCL and SRCL have a different parameter dependency because the coupling mechanism is different. The opto-mechanical coupling $\partial L_-/\partial l_\mathrm{p}, l_\mathrm{s}$ are in proportion to the arm power P_a and DARM offset ϵ. Therefore in total they scale with $P_\mathrm{in}^2 \epsilon^2$. This means that the couplings strongly depend on the laser power and DARM offset.

The PRCL coupling is weaker than that of SRCL by approximately two orders of magnitude. This is because the way they modulate the intensity of the arms are different. As discussed in sections 3.1 and 3.3, a deviation in SRCL directly modulates the amplitude of the large build-up field in the arms. In contrast, PRCL modulates the phase of the fields in the arms. The mechanical response provides a f^{-2} slope for SRCL and PRCL above 1 Hz and hence smaller couplings at higher frequencies.

In the rest of this section, we provide a brief review of the derivation of the radiation pressure couplings. As an example, we take a look at SRCL. According to equations (7), (14) and (15), Δl_s can displace the X and Y arms by

$$\Delta L_\mathrm{x} = -\Delta L_\mathrm{y} = \frac{16 P_\mathrm{a} r'_\mathrm{a} \epsilon g_\mathrm{s}^2 r_\mathrm{s}}{c s_\mu^2 t_\mathrm{s}^2 \left(1 + s_\mathrm{rse}\right)} k \Delta l_s. \tag{24}$$

As stated in [1, 2], our definition of DARM is given as $L_- = (L_\mathrm{x} - L_\mathrm{y})/2$. Therefore the resultant displacement in terms of the DARM degree-of-freedom can be calculated as

$$\frac{\partial L_-}{\partial l_\mathrm{s}} = \frac{1}{2}\left[\frac{\partial L_\mathrm{x}}{\partial l_\mathrm{s}} - \frac{\partial L_\mathrm{y}}{\partial l_\mathrm{s}}\right] = \frac{16 P_\mathrm{a} r'_\mathrm{a} \epsilon g_\mathrm{s}^2 r_\mathrm{s}}{c s_\mu^2 t_\mathrm{s}^2 \left(1 + s_\mathrm{rse}\right)} k. \tag{25}$$

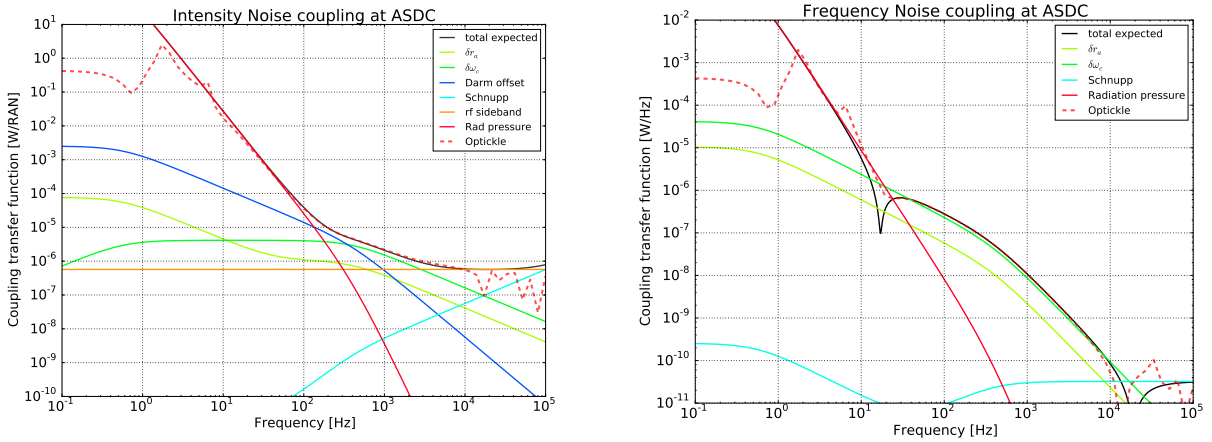

Figure 10: Intensity noise coupling (left) and frequency noise coupling (right).

Finally this displacement is read through the nominal DARM $\rightsquigarrow$ ASDC transfer function. The same analysis can be applied for $\Delta l_{\rm p}$ to obtain the coupling.

5 Laser noise couplings

The radiation pressure effect produces new coupling paths by physically displacing the DARM degree-of-freedom. Intensity, frequency and oscillator-amplitude noises primarily induce radiation pressure of the carrier field. On the other hand, oscillator-phase noise does not excite an audio sideband around the carrier and therefore increases the importance of the radiation pressure of the rf sidebands.

5.1 Intensity or amplitude noise

The coupling of intensity or amplitude noise can be summarized as

$$\begin{aligned}\frac{S^{(\rm int)}}{S_1} =& \left\{ \frac{\left[\left(1+r_{\rm a}\right) g_{\rm p} g_{\rm s} r'_{\rm a} \epsilon\right]^2}{\left(1+s_{cc}\right)\left(1+s_{rse}\right)} \right. \\ &+ \frac{\left(g_{\rm p} g_{\rm s}\right)^2 \delta r_{\rm a}}{\left(1+s_{cc}\right)\left(1+s_{rse}\right)} \left[\delta r_{\rm a} \left(1+s_c\right) + \frac{\delta\omega_{\rm c}}{\omega_{\rm c}} s_c \left(1+r_{\rm a}\right) - \frac{l_{\rm sch}\omega_{\rm c}}{c} r_{\rm a} s_{\rm c} \left(1-s_c/r_{\rm a}\right)\left(1+s_c\right) \right] \\ &\left. + 2T_{\rm omc} \left(\frac{J_1}{J_0} g_{\rm sb} t_{\rm sm}\right)^2 + 4 g_{\rm p}^2 g_{\rm s}^2 r'^2_{\rm a} \epsilon k \frac{1}{1+s_{\rm rse}} \left(A \frac{\partial L_-}{\partial A}\right) \right\} \left(\frac{\Delta A}{A}\right). \end{aligned} \tag{26}$$

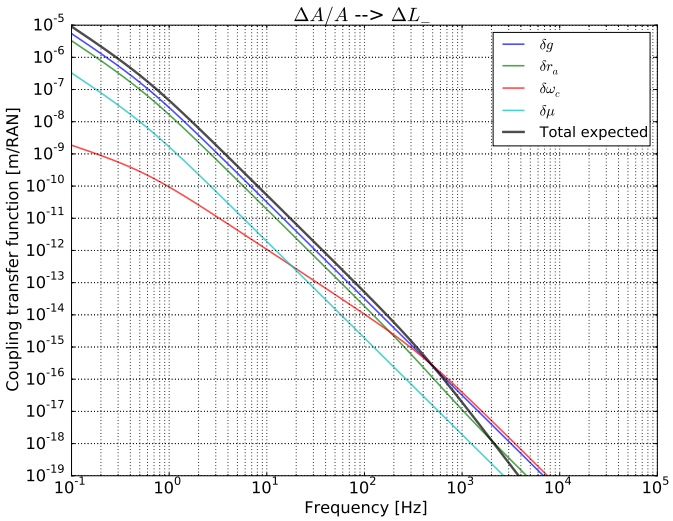

Figure 11: Transfer functions from relative amplitude noise $\Delta A/A$ to DARM displacement ΔL in [meters/RAN]. The numerical parameters for this calculation are listed in tables 1 and 2.

where the first three terms are the same as the non-radiation-pressure case [2]. The last term is the radiation pressure effect. The noise coupling transfer function is shown in figure 10. The opto-mechanical coupling coefficient, $A\partial L_-/\partial A$, is sensitive to imbalance between two arms. In fact, the coupling would disappear if the two arms were exactly identical. According to equation (20), the coupling coefficient can be expressed as,

$$A\frac{\partial L_-}{\partial A} = \frac{2P_\mathrm{a}}{cs_\mu^2\left(1+s_\mathrm{cc}\right)}\left[\left(\frac{\delta g}{g}\right)+\left(\frac{\delta\omega_\mathrm{c}}{\omega_\mathrm{c}}\right)\frac{g_\mathrm{s}s_\mathrm{c}\left(1-r_\mathrm{s}\right)}{t_\mathrm{s}\left(1+s_\mathrm{rse}\right)}-\delta r_\mathrm{a}\frac{g_\mathrm{s}r_\mathrm{s}\left(2+s_\mathrm{rse}\right)}{t_\mathrm{s}\left(1+s_\mathrm{rse}\right)}-2\left(\frac{\delta\mu}{\mu}\right)\right], \tag{27}$$

where we have added an extra coupling term due to a difference in the reduced mass between two arms $\delta\mu$ as pointed out by Somiya in [7]. An example coupling is shown in figure 11 together with individual components. The opto-mechanical coupling scales with the arm power P_a and is filtered as $1/f^3$ by the mechanical response as well as the CARM cavity pole.

The coupling term associated with the reduced mass can be derived as follows. First of all, when the reduced masses are different between two arms, they are going to be displaced by different amount when an identical amount of force is exerted. In this case, the resultant

DARM displacement can be calculated by

$$\begin{aligned}\Delta L_- =& -\frac{1}{2}\left(\frac{2\Delta P_{\rm x}}{c\left(\mu+\delta\mu\right)\omega^2}-\frac{2\Delta P_{\rm y}}{c\left(\mu-\delta\mu\right)\omega^2}\right)\\ \approx& -\frac{4P_{\rm a}}{cs_\mu^2\left(1+s_{\rm cc}\right)}\left(\frac{\delta\mu}{\mu}\right)\left(\frac{\Delta A}{A}\right),\end{aligned} \tag{28}$$

where we have used equation (20) and expanded $\delta\mu$ to first order.

Note that reference [7] considers loss on the beam splitter in addition. It can be handled as a proper combination of δg and $\delta r_{\rm a}$ in our case.

5.2 Frequency noise

The coupling can be written as,

$$\begin{aligned}\frac{S^{(\rm freq)}}{S_1} =& \frac{\left(1+r_{\rm a}\right)\left(g_{\rm p}g_{\rm s}\right)^2 r'_{\rm a}\epsilon}{\left(1+s_{cc}\right)\left(1+s_{\rm rse}\right)}\left[-\delta r_{\rm a}-\frac{\delta\omega_{\rm c}}{\omega_{\rm c}}\left(1+r_{\rm a}\right)+\frac{l_{\rm sch}\omega_{\rm c}r_{\rm a}}{c}\left(1-s_c/r_{\rm a}\right)\left(1+s_c\right)\right]\left(\frac{2\pi\Delta f}{\omega_{\rm c}}\right)\\ &+4g_{\rm p}^2g_{\rm s}^2r_{\rm a}'^2\epsilon k\frac{1}{1+s_{\rm rse}}\left(\frac{\partial L_-}{\partial f}\right)\Delta f\end{aligned} \tag{29}$$

where we have omitted the CARM offset term [2] but kept the other terms. The only difference is the radiation pressure coupling. $\partial L_-/\partial f$ is the radiation pressure coupling given by

$$\frac{\partial L_-}{\partial f} = -\frac{8\pi P_{\rm a}g_{\rm s}^2r'_{\rm a}\epsilon}{J_0c\omega_{\rm rse}s_\mu^2\left(1+s_{\rm cc}\right)\left(1+s_{\rm rse}\right)}. \tag{30}$$

The response is shown in figure 10. Despite the sign mystery in the intensity fluctuation (see section 3.2), the transfer functions agree with Optickle. Currently this issue is under investigation.

5.3 Oscillator amplitude noise

The coupling of oscillator amplitude noise is similar to that of laser amplitude noise. A small deviation in the modulation depth produces a pair of amplitude-modulation sidebands around the carrier and rf sidebands simultaneously. The way these two pairs of audio sidebands couple to AS DC is the same as intensity noise except that the scaling factor is

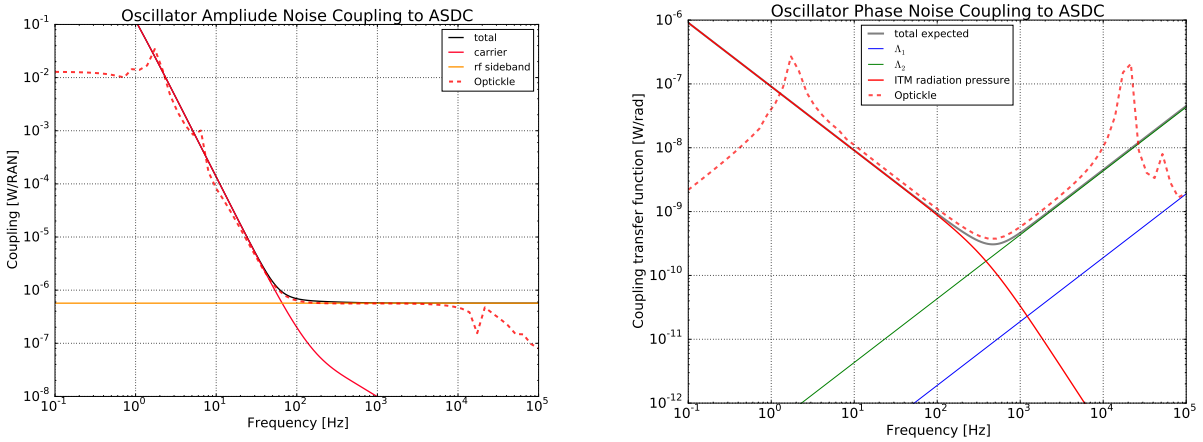

Figure 12: Oscillator amplitude noise coupling (left) and oscillator phase noise coupling (right).

different. The coupling can be summarized as,

$$\begin{aligned}\frac{S^{(\mathrm{osc,\,a})}}{S_1} = &-\frac{\Gamma^2}{2}\Bigg\{\frac{\left[\left(1+r_\mathrm{a}\right)g_\mathrm{p}g_\mathrm{s}r'_\mathrm{a}\epsilon\right]^2}{\left(1+s_{cc}\right)\left(1+s_{rse}\right)}\\ &+\frac{\delta r_\mathrm{a}\left(g_\mathrm{p}g_\mathrm{s}\right)^2}{\left(1+s_{cc}\right)\left(1+s_{rse}\right)}\left[\delta r_\mathrm{a}\left(1+s_c\right)+\delta\omega_\mathrm{c}s_c\left(1+r_\mathrm{a}\right)-\frac{l_\mathrm{sch}\omega_\mathrm{c}}{c}r_\mathrm{a}\left(1-s_cr_\mathrm{a}\right)\left(1+s_c\right)\right]\\ &-T_\mathrm{omc}\left(\frac{g_\mathrm{sb}t_\mathrm{sm}}{J_0}\right)^2+4g_\mathrm{p}^2g_\mathrm{s}^2r_\mathrm{a}'^2\epsilon k\frac{1}{1+s_\mathrm{rse}}\left(A\frac{\partial L_-}{\partial A}\right)\Bigg\}\left(\frac{\Delta\Gamma}{\Gamma}\right).\end{aligned} \tag{31}$$

The first two and last terms are the carrier component that has the same function form as intensity noise but an extra attenuation factor of $-\Gamma^2/2$. Figure 12 shows the coupling transfer function in bode plot.

5.4 Oscillator phase noise

The coupling of oscillator phase noise is perhaps the most complicated one among all laser noises. The coupling was found to be quite sensitive to a mismatch between the cavity lengths and rf sideband frequency. We define the mismatch for the arm cavities as

$$\Delta\Phi_\mathrm{a} = \mathbf{mod}\left(\frac{\omega_\mathrm{m}L}{c},\frac{\pi}{4}\right). \tag{32}$$

When $\Delta\Phi_{\rm a}$ is zero, it means that the rf sideband is exactly on an anti-resonance point. The size of $\Delta\Phi_{\rm a}$ represents how far away the rf sideband is from the exact resonance in terms of the single trip phase in radians. In practice, we design the mismatch to be a small, but non zero value in order to avoid undesired resonance of the higher harmonics. For example, $\Delta\Phi_{\rm a}$ in aLIGO is 0.1 rad (see table 2).

The noise coupling transfer function can be written as,

$$\begin{aligned}\frac{S^{(\rm dc)}}{S_1} =& \Bigg[2T_{\rm omc}\frac{\left(J_1 g_{\rm sb} t_{\rm sm}\right)^2 s_{\rm c}\omega_{\rm c}\Lambda_1}{cJ_0^2\sin\phi_{\rm sch}} - 8T_{\rm omc}\hat{r_{\rm a}}'\Delta\Phi_{\rm a}\frac{J_1^2\left(g_{\rm sb}t_{\rm sm}\right)^4 s_{\rm c}\omega_{\rm c}\Lambda_2}{c\left(J_0\hat{r_{\rm a}}t_{\rm p}t_{\rm s}\sin\phi_{\rm sch}\right)^2} \\ &+ 4g_{\rm p}^2 g_{\rm s}^2 r_{\rm a}'^2\epsilon k\frac{1}{1+s_{\rm rse}}\left(\frac{\partial L_-}{\partial\Phi}\right)\Bigg]\Delta\Phi.\end{aligned} \tag{33}$$

where Λ_1 and Λ_2 are coupling coefficients in unit of length. They are defined as,

$$\begin{aligned}\Lambda_1 =& l_{\rm sch}\frac{\cos\phi_{\rm sch} + \left(r_{\rm p}+r_{\rm s}\right)\hat{r_{\rm a}} + r_{\rm p}r_{\rm s}\hat{r_{\rm a}}^2\cos\phi_{\rm sch}}{1+\hat{r_{\rm a}}\left(r_{\rm p}+r_{\rm s}\right)\cos\phi_{\rm sch} + r_{\rm p}r_{\rm s}\hat{r_{\rm a}}^2}, \\ \Lambda_2 =& \left[\left(l_{\rm p}r_{\rm s}+l_{\rm s}r_{\rm p}\right)r_{\rm p}r_{\rm s}\hat{r_{\rm a}}^2\cos\phi_{\rm sch} + 2r_{\rm p}r_{\rm s}\hat{r_{\rm a}}\left(l_{\rm p}+l_{\rm s}\right) + \left(l_{\rm s}r_{\rm s}+l_{\rm p}r_{\rm p}\right)\cos\phi_{\rm sch}\right].\end{aligned} \tag{34}$$

Also, $\partial L_-/\partial\Phi$ is a radiation pressure coupling coefficient given as,

$$\frac{\partial L_-}{\partial\Phi} = -\frac{\left(2J_1 g_{\rm sb}t_{\rm sm}\right)^2 r_{\rm s}}{cs_\mu^2\hat{r_{\rm a}}t_{\rm s}^2\sin\phi_{\rm sch}}\frac{\omega}{c}\left(l_{\rm s} - L\frac{\hat{r_{\rm a}}'}{\hat{r_{\rm a}}}\right). \tag{35}$$

This coupling is due to the radiation pressure of the rf sidebands acting on the AR side of ITMs. An interesting point is that this particular radiation pressure coupling would vanish if SRM was removed. When SRM does not exist, the audio sidebands around the rf sidebands mostly behave as phase modulation in the power recycling cavity and therefore do not impose intensity variation at ITMs. On the other hand, when the rf sidebands exit the interferometer through the Michelson interferometer, a phase-to-amplitude conversion happens due to the Schnupp asymmetry (as a function of the modulation frequency). Therefore once we put SRM back in place, it recycles these amplitude modulated rf sidebands back into the interferometer and consequently produces intensity variation at ITMs. In addition, there is an enhancement effect due to the finite length of the signal recycling cavity. When the signal recycled field arrives at an ITM and interferes with the power recycling cavity field, they don't exactly interfere in the constructive manner even if the PRC and SRC lengths are

perfectly matched to the resonant conditions. The constructive interference monotonically degrades as the frequency goes higher because the signal recycling field picks up an extra phase delay simply due to its propagation. Therefore the opto-mechanical coupling depends on the propagation delay $\omega l_s/c$. Similarly, the arm cavities introduces the same effect and hence an extra dependency $\omega L/c$.

Additionally, we should mention that the macroscopic length of PRCL and SRCL can also change the coupling in a similar manner to the arm mismatch $\Delta\Phi_a$. This effect is not included in the calculation.

6 Conclusions and prospects

We have derived a set of analytic equations that describe the frequency responses of the aLIGO interferometer with the DC readout and radiation pressure effects incorporated. We have confirmed that the DARM offset permits various noises to couple to the DC readout through the radiation pressure effect. Since the effects are significant at low frequencies and therefore they are critical when considering noise couplings.

In the next part of the study, we plan to properly incorporate the phase rotation of the audio sidebands in the Schnupp asymmetry which has been often neglected. It is expected to produce quadrature-phase signals for CARM, PRCL and SRCL which have been thought to be purely on in-phase and hence another complexity in the length sensing.

A Numerical parameters

symbol	description	value
	Optical properties	
$T_{\rm i}$	ITM power transmissivity	0.0140
$\lambda_{\rm i}$	ITM loss on the HR surface	0
$t_{\rm i}$	ITM amplitude transmissivity or $\sqrt{T_{\rm i}}$	
$r_{\rm i}$	ITM amplitude reflectivity or $\sqrt{1-T_{\rm i}-\lambda_{\rm i}}$	
$T_{\rm e}$	ETM power trasmissivity	50e-6
$\lambda_{\rm e}$	ETM loss on the HR surface	0
$t_{\rm e}$	ETM amplitude transmissivity or $\sqrt{T_{\rm e}}$	
$r_{\rm e}$	ETM amplitude reflectivity or $\sqrt{1-T_{\rm e}-\lambda_{\rm e}}$	
$T_{\rm p}$	PRM power trasmissivity	0.031
$\lambda_{\rm p}$	PRM loss on the HR surface	0
$t_{\rm p}$	PRM amplitude transmissivity or $\sqrt{T_{\rm p}}$	
$r_{\rm p}$	PRM amplitude reflectivity or $\sqrt{1-T_{\rm p}-\lambda_{\rm p}}$	
$T_{\rm s}$	SRM power trasmissivity	0.35
$\lambda_{\rm s}$	SRM loss on the HR surface	0
$t_{\rm s}$	SRM amplitude transmissivity or $\sqrt{T_{\rm s}}$	
$r_{\rm s}$	SRM amplitude reflectivity or $\sqrt{1-T_{\rm s}-\lambda_{\rm s}}$	
$T_{\rm omc}^{\rm (c)}$	OMC transmittance for the carrier	1
$T_{\rm omc}^{\rm (sb1)}$	OMC transmittance for the f_1 sidebands	not in use
$T_{\rm omc}^{\rm (sb2)}$	OMC transmittance for the f_2 sidebands	61.4 ppm
	optical distances	
$L_{\rm arm}$	arm length (both X and Y)	3994.5 m
$l_{\rm sch}$	Schnupp asymmetry or $l_{\rm x}-l_{\rm y}$	0.08 m
$l_{\rm p}$	Power recycling cavity length	57.651 m
$l_{\rm s}$	Signal recycling cavity length	56.004 m
L_ϵ	DARM offset	5 pm
	Laser property	
$P_{\rm in}$	input laser power	125 W
f_1	modulation frequency of the first rf sideband	9100230 Hz
f_2	modulation frequency of the second rf sideband	45501150 Hz
Γ_1	modulation depth of the f_1 rf sideband	0.1 rad
Γ_2	modulation depth of the f_2 rf sideband	0.1 rad
	Mechanical property	
m	mass of ETMs and ITMs	39.5 kg
$m_{\rm bs}$	mass of BS	14.2 kg
$m_{\rm pr}$	mass of PRM	2.92 kg
$m_{\rm pr2}$	mass of PR2	3.15 kg
$m_{\rm sr}$	mass of SRM	2.92 kg

Table 1: Summary of the numerical parameters for the length responses. No losses or imbalance are introduced for simplicity. Note that PR3, SR2 and SR3 do not exist in either numerical simulation or analytic calculation.

symbol	description	value
	ITM properties	
δT_i	difference in ITM power transmissivity	100 ppm
λ_i	ITM loss on the HR surface	0
T_ix	ITMX power transmissivity $T_\mathrm{i} + \delta T_\mathrm{i}$	0.141
T_iy	ITMY power transmissivity $T_\mathrm{i} - \delta T_\mathrm{i}$	0.139
t_ix	ITMX amplitude transmissivity or $\sqrt{T_\mathrm{ix}}$	
t_iy	ITMY amplitude transmissivity or $\sqrt{T_\mathrm{iy}}$	
r_ix	ITMX amplitude reflectivity or $\sqrt{1 - T_\mathrm{i} - \delta T_\mathrm{i}}$	
r_iy	ITMY amplitude reflectivity or $\sqrt{1 - T_\mathrm{i} + \delta T_\mathrm{i}}$	
m_ix	ITMX mass	39.589 kg
m_iy	ITMY mass	39.636 kg
	ETM properties	
λ_e	ETM loss on the HR surface	30 ppm
$\delta\lambda_\mathrm{e}$	ETM differential loss on the HR surface	-20 ppm
r_ex	ETMX amplitude reflectivity or $\sqrt{1 - T_\mathrm{e} - \lambda_\mathrm{e} - \delta\lambda_\mathrm{e}}$	
r_ey	ETMY amplitude reflectivity or $\sqrt{1 - T_\mathrm{e} - \lambda_\mathrm{e} + \delta\lambda_\mathrm{e}}$	
m_ex	ETMX mass	39.603 kg
m_ey	ETMY mass	39.597 kg
	Arm cavity properties	
$\omega_\mathrm{c}^{(\mathrm{xarm})}/(2\pi)$	X arm cavity pole	42.5842 Hz
$\omega_\mathrm{c}^{(\mathrm{yarm})}/(2\pi)$	Y arm cavity pole	42.0980 Hz
$\delta\omega_\mathrm{c}/(2\pi)$	Difference in the cavity pole frequency or $(\omega_\mathrm{c}^{(\mathrm{xarm})} - \omega_\mathrm{c}^{(\mathrm{yarm})})/(4\pi)$	0.24313 Hz
$r_\mathrm{a}^{(\mathrm{xarm})}$	X arm reflectivity for the carrier light	0.99159
$r_\mathrm{a}^{(\mathrm{yarm})}$	Y arm reflectivity for the carrier light	0.985812
δr_a	Difference in arm reflectivity or $(r_\mathrm{a}^{(\mathrm{xarm})} - r_\mathrm{a}^{(\mathrm{xarm})})/2$	0.002886
μ_x	Reduced mass of X arm or $m_\mathrm{ix} m_\mathrm{ex}/(m_\mathrm{ix} + m_\mathrm{ex})$	19.80 kg
μ_y	Reduced mass of Y arm or $m_\mathrm{iy} m_\mathrm{ey}/(m_\mathrm{iy} + m_\mathrm{ey})$	19.81 kg
$\delta\mu$	Difference in the reduced masses or $(\mu_\mathrm{x} - \mu_\mathrm{y})/2$	-5.123 g
δg	Difference in the arm gain or $(g_\mathrm{x} - g_\mathrm{y})/2$	-0.036
$\Delta\Phi_\mathrm{arm}$	Mismatch for the 45 MHz rf sidebands or $\mathbf{mod}(2\pi f_2 L_\mathrm{arm}/c, \pi/4)$	108.30 mrad

Table 2: Summary of the numerical parameters for the laser noise couplings. Loss is added to ETMs. ITMs have different reflectivity. The rest of parameters are unchanged from table 1

.

References

[1] K. Izumi and D. Sigg,"Frequency response of the aLIGO interferometer: part 1", LIGO-T1500461(2015)
https://dcc.ligo.org/LIGO-T1500325

[2] K. Izumi , D. Sigg and K. Kawabe,"Frequency response of the aLIGO interferometer: part 2", LIGO-T1500461(2015)
https://dcc.ligo.org/LIGO-T1500461

[3] Optickle is a matlab-based frequency domain numerical simulator developed by M. Evans
https://github.com/Optickle/Optickle

[4] Martin Regehr, "Signal Extraction and Control for an Interferometric Gravitational Wave Detector", Thesis, Caltech (1995)

[5] Thomas Corbitt, "Quantum Noise and Radiation Pressure Effects in High Power Optical Interferometers", Massachusetts Institute of Technology (2008)
https://gwic.ligo.org/thesisprize/2008/Corbitt_Thesis.pdf

[6] Haixing Miao, "Exploring Macroscopic Quantum Mechanics in Optomechanical Devices", The University of Western Australia (2010)
https://gwic.ligo.org/thesisprize/2010/miao_thesis.pdf

[7] K. Somiya and et al. "Frequency noise and intensity noise of next-generation gravitational-wave detectors with RF/DC readout schemes", Phys. Rev. D 73 122005 (2006)
http://journals.aps.org/prd/abstract/10.1103/PhysRevD.73.122005